Supporting Information

Sea Urchin-Like Ni-Fe Sulfides Architecture as Efficient Electrocatalysts for the Oxygen Evolution Reaction

*Cuijuan Xuan[a], Wen Lei[a], Jie Wang[b], Tonghui Zhao[a], Chenglong Lai[a], Ye Zhu[b], Yubao Sun[c], Deli Wang[a]**

[a] Key laboratory of Material Chemistry for Energy Conversion and Storage (Huazhong University of Science and Technology), Ministry of Education, Hubei Key Laboratory of Material Chemistry and Service Failure, School of Chemistry and Chemical Engineering, Huazhong University of Science and Technology, Wuhan 430074, China.

[b] Department of Applied Physics, The Hong Kong Polytechnic University, Hung Horn, Kowloon, Hong Kong.

[c] Faculty of Material Science and Chemistry, China University of Geosciences (Wuhan), Wuhan 430074, China.

* E-mail: wangdl81125@hust.edu.cn

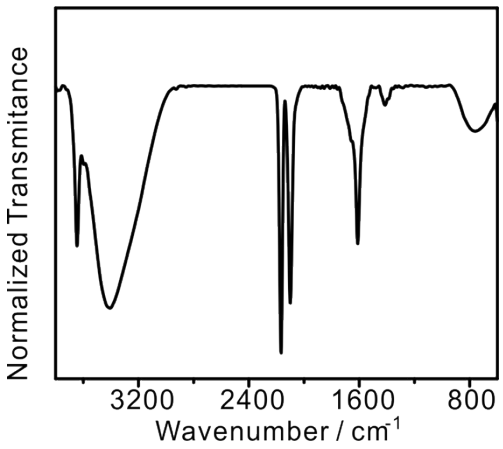

Figure S1 FT-IR spectrum of NiFe-PBA.

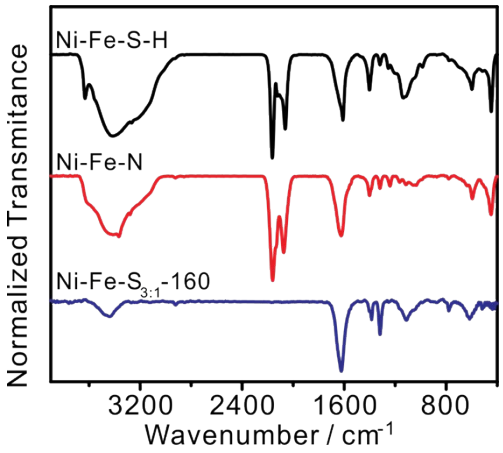

Figure S2 FT-IR spectra of Ni-Fe-S-H, Ni-Fe-N, and Ni-Fe-$S_{3:1}$-160.

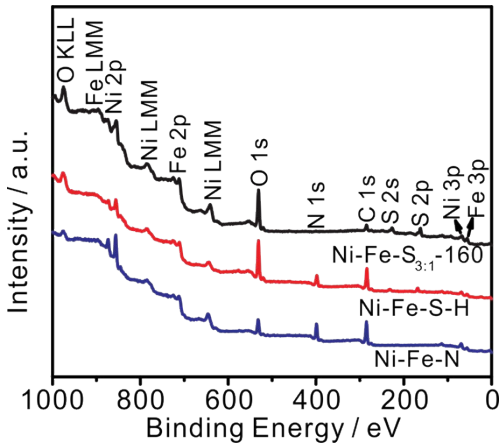

Figure S3 XPS survey spectra of Ni-Fe-S-H, Ni-Fe-N, and Ni-Fe-$S_{3:1}$-160.

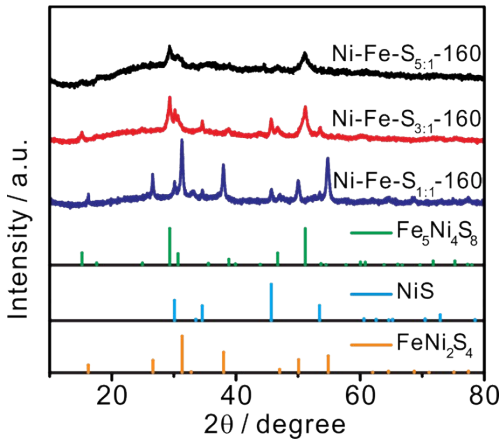

Figure S4 XRD patterns of the materials prepared under different mass ratio of NiFe-PBA and S powder.

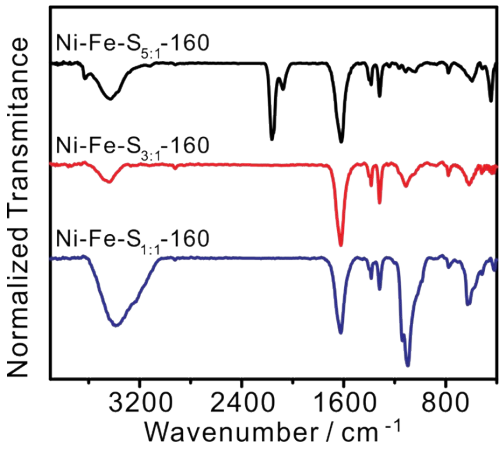

Figure S5 FT-IR spectra of the materials prepared under different mass ratio of NiFe-PBA and S powder.

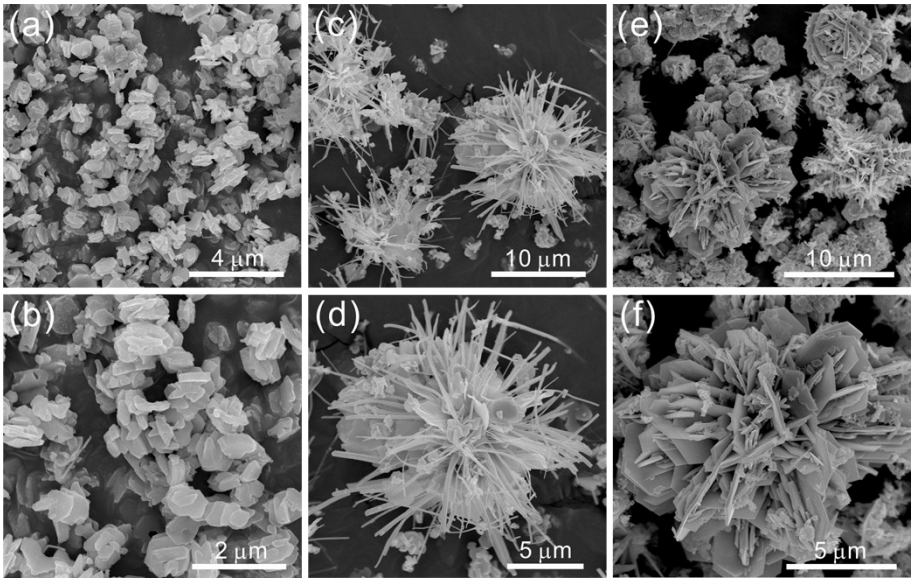

Figure S6 SEM images of the materials prepared under the mass ratio of NiFe-PBA and S powder for (a, b) 5:1, (c, d) 3:1, and (e, f) 1:1.

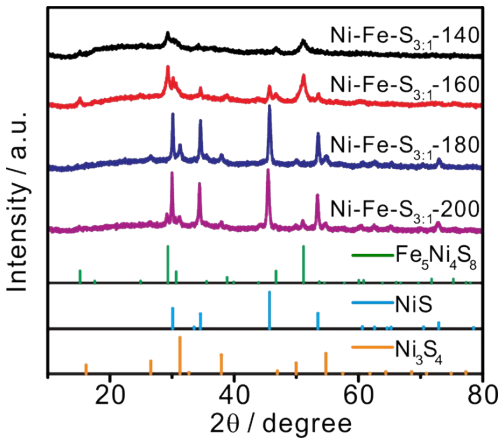

Figure S7 XRD patterns of the materials prepared under different hydrothermal temperature.

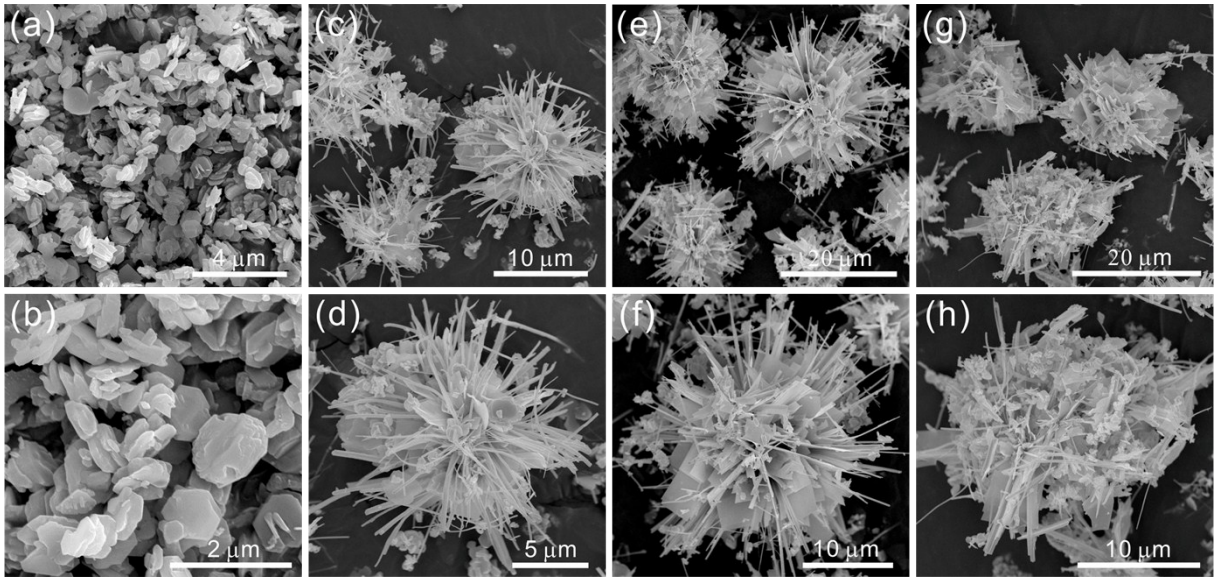

Figure S8 SEM images of the materials prepared under the hydrothermal temperature of (a, b) 140 °C, (c, d) 160 °C, (e, f) 180 °C, and (g, h) 200 °C.

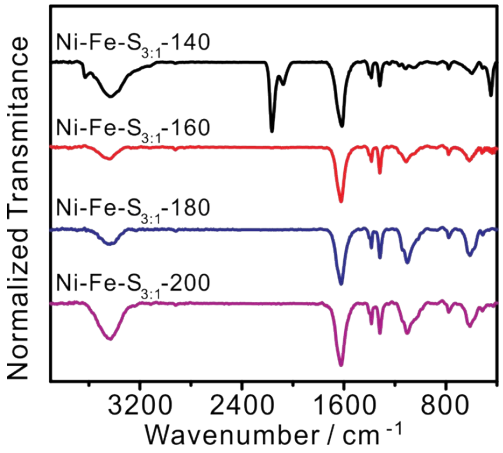

Figure S9 FT-IR spectra of the materials prepared under different hydrothermal temperature.

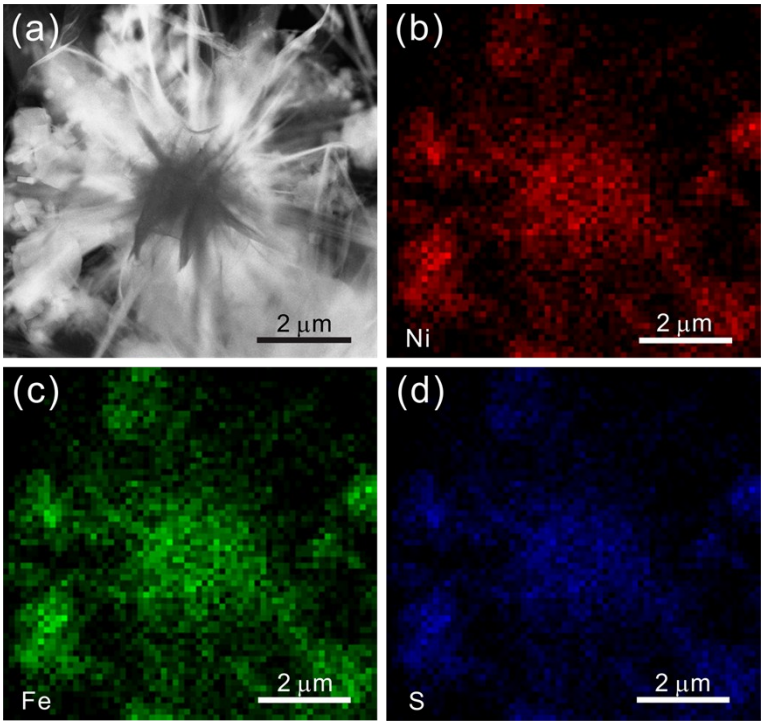

Figure S10 (a) S-TEM image of Ni-Fe-$S_{3:1}$-160 and the corresponding elemental mapping of (b) Ni, (c) Fe and (d) S.

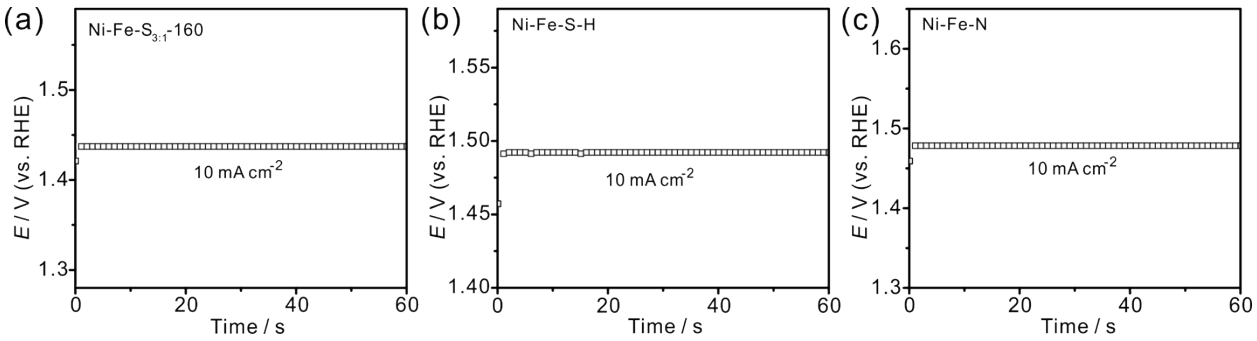

Figure S11 Chronopotentiometric responses for Ni-Fe-$S_{3:1}$-160, Ni-Fe-S-H, and Ni-Fe-N at a constant current density of 10 mA cm^{-2}.

The determination of the overpotential at 10 mA cm^2 based on the LSV curve of Ni-Fe-$S_{3:1}$-160 is not very accurate due to its obvious oxidation peak, so chronopotentiometry measurements were performed for 60 s to obtain the overpotential at 10 mA cm^{-2} (η_{10}). The results show that the η_{10} for Ni-Fe-$S_{3:1}$-160, Ni-Fe-S-H, Ni-Fe-N is 207, 262, and 249 mV respectively.

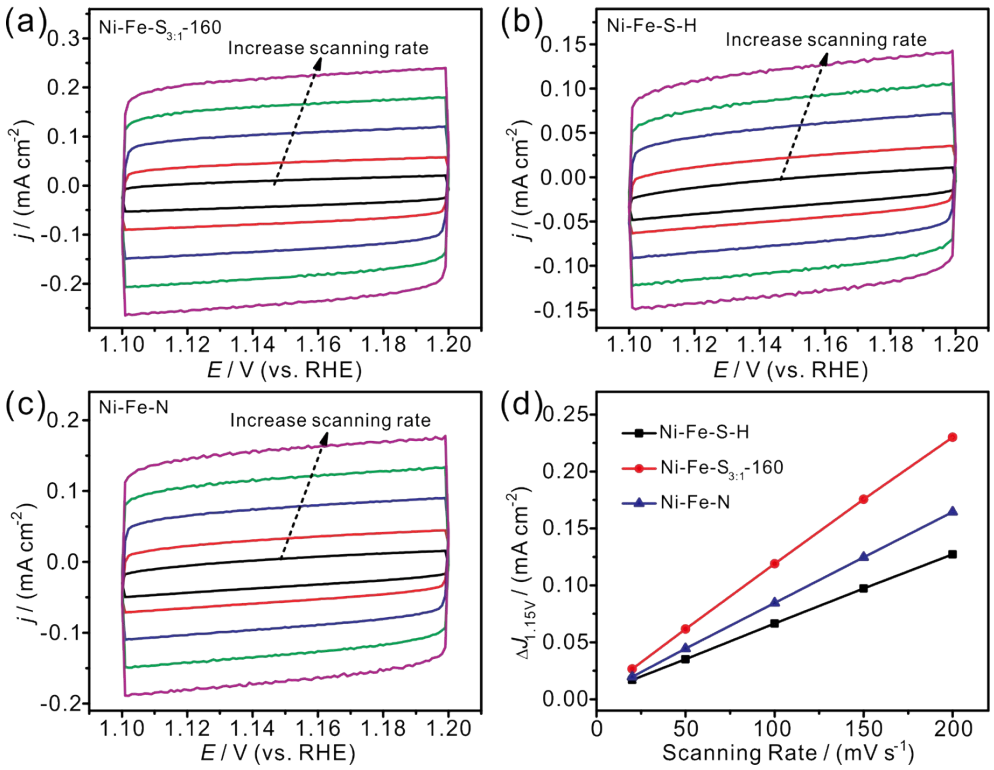

Figure S12 CV curves at various scan rates (20, 50, 100, 150 mV s^{-1}) of Ni-Fe-$S_{3:1}$-160 (a), Ni-Fe-S-H (b), and Ni-Fe-N (c). (d) Plots of the half of current density variation (ΔJ = (/*J*a/ + /*J*c/)/2) at 1.15 V versus scan rates for Ni-Fe-$S_{3:1}$-160, Ni-Fe-S-H, and Ni-Fe-N.

CV measurements were performed at various scan rates in the potential between 1.1 to 1.2 V (Figure R2a-c) and the half of the difference of the positive and negative current density (ΔJ) at 1.15 V against the scan rate is plotted (Figure R2d) to obtain the slope which is the C_{dl}.

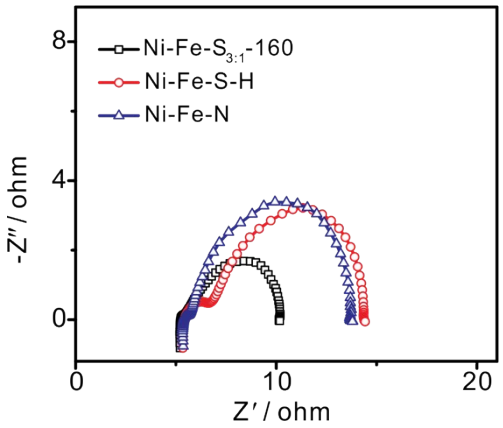

Figure S13 Nyquist plots of Ni-Fe-S-H, Ni-Fe-N, and Ni-Fe-$S_{3:1}$-160 at the potential of 1.5 V in the frequency ranging from 100 kHz to 0.01 Hz.

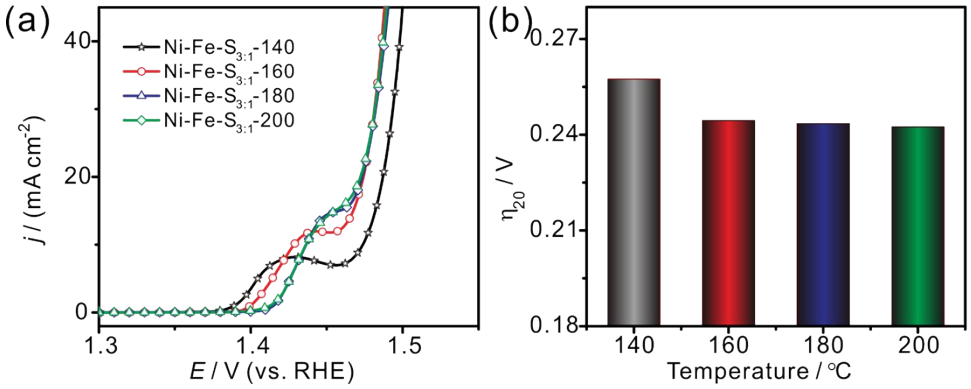

Figure S14 (a) LSV curves of the materials prepared at different hydrothermal temperatures, and (b) the corresponding overpotential at a current density of 20 mA cm^{-2}.

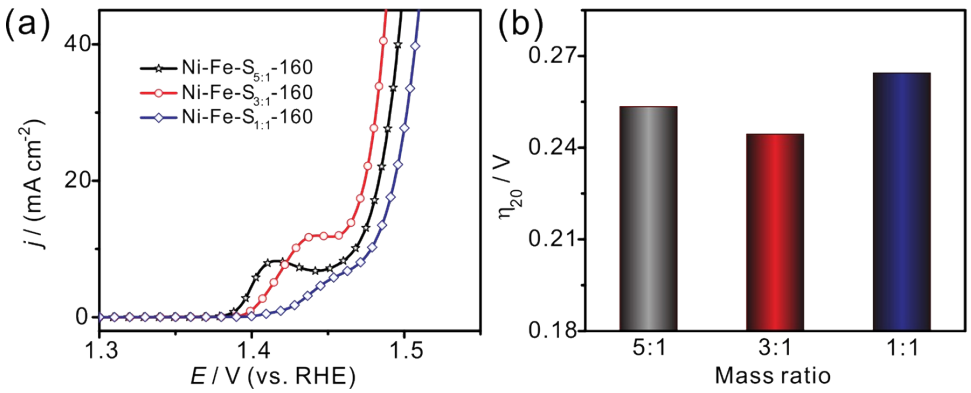

Figure S15 (a) LSV curves of the materials prepared at different mass ratio of NiFe-PBA and S powder, and (b) the corresponding overpotential at a current density of 20 mA cm^{-2}.

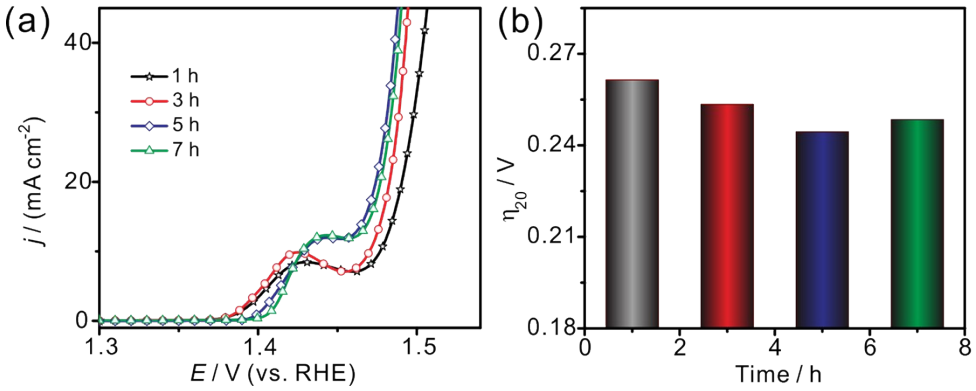

Figure S16 (a) LSV curves of the materials prepared at different hydrothermal time, and (b) the corresponding overpotential at a current density of 20 mA cm^{-2}.

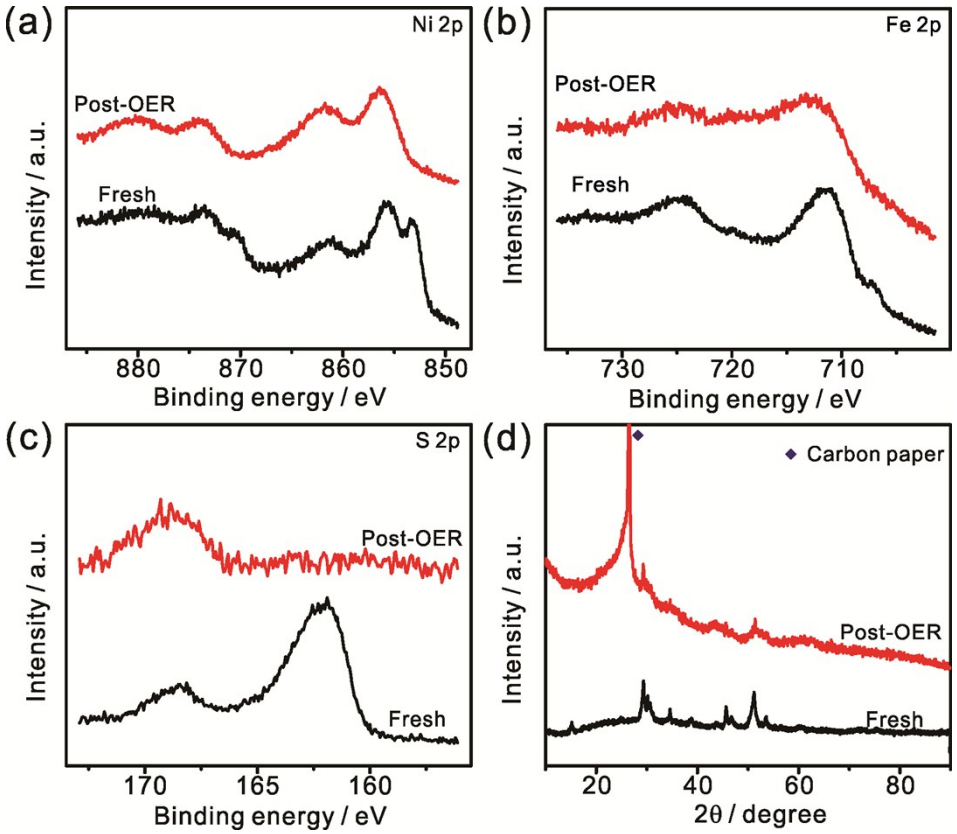

Figure S17 High-resolution Ni 2p (a), and Fe 2p (b), S 2p (c) XPS spectra for fresh, and post-OER Ni-Fe-$S_{3:1}$-160 samples. (d) XRD patterns of Ni-Fe-$S_{3:1}$-160 after 3000 CV cycles in the potential range from 1.4 V to 1.8 V for OER.

Table S1 Comparison of OER catalytic performance of transition metal-based sulfides reported in literature.

Catalyst	Support	Electrolyte	Loading (mg cm^{-2})	j (mA cm^{-2})	Overpotential (mV)	Refs
Ni_3S_2/NF	Ni foam	1.0 M NaOH	~1.6	10	260	[1]
Ultrathin Co_3S_4 Nanosheets	GCE	0.1 M KOH	0.28	10	355	[2]
Co_9S_8@MoS_2/carbon nanofibers	GCE	1.0 M KOH	0.212	10	≈430	[3]
Carbon paper/carbon tubes/cobalt-sulfide sheets	carbon paper	1.0 M KOH	~0.32	10	306	[4]
$NiCo_2S_4$ nanowire arrays/Ni foam	Ni foam	1.0 M KOH	—	10	260	[5]
Co_9S_8/graphene hybrid	GCE	0.1 M KOH	0.2	10	409	[6]
Nickel(II) sulfide (NiS) nanosheets	stainless steel meshes	0.1 M KOH	~1	10	297	[7]
Nickel sulfide (NiS_x)	Si wafer substrates	1.0 M KOH	—	10	372	[8]
$Co_{1-x}S$/N and S co-doped graphene nanoholes	GCE	0.1 M KOH	0.5	10	371	[9]
Oxygen-incorporated amorphous cobalt sulfide porous nanocubes	GCE	1.0 M KOH 0.1 M phosphate buffer solution	0.8	10 4.59	290 570	[10]
Hierarchical Co_9S_8 hollow microplates	GCE	1.0 M KOH	0.37	10	278	[11]
NGO/Ni_7S_6	GCE	0.1 M KOH	0.21	10	380	[12]
$CuCo_2S_4$	GCE	1 M KOH	0.7	10	310	[13]
Amorphous $CoS_{4.6}O_{0.6}$ porous nanocubes	GCE	1 M KOH	0.8	10	290	[10]
Co_9S_8/CNT/carbon cloth	carbon cloth	0.1 M KOH	0.5	10	321	[14]
TiO_2@Co_9S_8	Ni foam	1 M KOH	—	10	240	[15]
Co_9S_8@MoS_2	GCE	1 M KOH	0.41	10	340	[16]

Co-MoS_2/bacterial cellulose-derived carbon fibers	carbon fiber paper	1 M KOH	2	10	260	[17]
$NiS_{1.03}$-N and S co-doped carbon nanoparticles	carbon cloth	1 M KOH	0.25	10	270	[18]
Co_9S_8	carbon fibre paper	1 M KOH	1.7	10	288	[19]
Cu_2S/Cu foam	Cu foam	1 M KOH	—	20	336	[20]
Cobalt sulfide/carbon composites	GCE	0.1 M KOH	~0.57	10	302	[21]
$FeNi_2S_4$ hollow balloons	Ni foam	1.0 M KOH	0.6	10	273	[22]
CeO_x/CoS	GCE	1.0 M KOH	0.20	10	269	[23]
Co_3S_4@MoS_2	GCE	1.0 M KOH	0.283	10	280	[24]
CoeNieS@N, S-doped porous carbon	GCE	0.1 M KOH	0.39	10	470	[25]
Ni@NiS_2@S/N-doped hollow carbon capsules	GCE	0.1 M KOH	0.10	10	440	[26]
$Co_xNi_{1-x}S_2$-rGO	GCE	1.0 M KOH	0.285	10	290	[27]
(Ni, Fe)S_2@MoS_2	carbon fiber paper	1.0 M KOH	—	10	270	[28]
N-$NiMoO_4$/NiS_2	GCE	1.0 M KOH	0.20	10	267	[29]
Ni-Fe-$S_{3:1}$-160	GCE	1.0 M KOH	0.42	10 20	207 245	This work

References

1 L.-L. Feng, G. Yu, Y. Wu, G.-D. Li, H. Li, Y. Sun, T. Asefa, W. Chen and X. Zou, *J. Am. Chem. Soc*, 2015, **137**, 14023-14026.

2 Y. Liu, C. Xiao, M. Lyu, Y. Lin, W. Cai, P. Huang, W. Tong, Y. Zou and Y. Xie, *Angew. Chem.*, 2015, **127**, 11383-11387.

3 H. Zhu, J. Zhang, R. Yanzhang, M. Du, Q. Wang, G. Gao, J. Wu, G. Wu, M. Zhang and B. Liu, *Adv. Mater.*, 2015, **27**, 4752-4759.

4 J. Wang, H.-x. Zhong, Z.-l. Wang, F.-l. Meng and X.-b. Zhang, *ACS nano*, 2016, **10**, 2342-

2348.

5 A. Sivanantham, P. Ganesan and S. Shanmugam, *Adv. Funct. Mater.*, 2016, **26**, 4661-4672.

6 S. Dou, L. Tao, J. Huo, S. Wang and L. Dai, *Energy Environ. Sci.*, 2016, **9**, 1320-1326.

7 J. S. Chen, J. Ren, M. Shalom, T. Fellinger and M. Antonietti, *ACS Appl. Mater. Interfaces*, 2016, **8**, 5509-5516.

8 H. Li, Y. Shao, Y. Su, Y. Gao and X. Wang, *Chem. Mater.*, 2016, **28**, 1155-1164.

9 X. Qiao, J. Jin, Y. Li and S. Liao, *J. Mater. Chem. A*, 2017, **5**, 12354-12360.

10 P. Cai, J. Huang, J. Chen and Z. Wen, *Angew. Chem. Int. Ed.*, 2017, **56**, 4858-4861.

11 H. Liu, F.-X. Ma, C.-Y. Xu, L. Yang, Y. Du, P.-P. Wang, S. Yang and L. Zhen, *ACS Appl. Mater. Interfaces*, 2017, **9**, 11634-11641.

12 K. Jayaramulu, J. Masa, O. Tomanec, D. Peeters, V. Ranc, A. Schneemann, R. Zboril, W. Schuhmann and R. A. Fischer, *Adv. Funct. Mater.*, 2017, **27**, 1700451.

13 M. Chauhan, K. P. Reddy, C. S. Gopinath and S. Deka, *ACS Catal.*, 2017, **7**, 5871-5879.

14 H. Li, Z. Guo and X. Wang, *J. Mater. Chem. A*, 2017, **5**, 21353-21361.

15 S. Deng, Y. Zhong, Y. Zeng, Y. Wang, X. Wang, X. Lu, X. Xia and J. Tu, *Adv. Sci.*, 2018, **5**, 1700772.

16 J. Bai, T. Meng, D. Guo, S. Wang, B. Mao and M. Cao, *ACS Appl. Mater. Interfaces*, 2018, **10**, 1678-1689.

17 Q. Xiong, Y. Wang, P. F. Liu, L. R. Zheng, G. Wang, H. G. Yang, P. K. Wong, H. Zhang and H. Zhao, *Adv. Mater.*, 2018, 1801450.

18 H. Yang, C. Wang, Y. Zhang and Q. Wang, *Small*, 2018, **14**, 1703273.

19 R. Souleymen, Z. Wang, C. Qiao, M. Naveed and C. Cao, *J. Mater. Chem. A*, 2018, **6**, 7592-7607.

20 L. He, D. Zhou, Y. Lin, R. Ge, X. Hou, X. Sun and C. Zheng, *ACS Catal.*, 2018, **8**, 3859-3864.

21 Z. Chen, R. Wu, M. Liu, Y. Liu, S. Xu, Y. Ha, Y. Guo, X. Yu, D. Sun and F. Fang, *J. Mater. Chem. A*, 2018, **6**, 10304-10312.

22 H. Wang, J. Tang, Y. Li, H. Chu, Y. Ge, R. Baines, P. Dong, P. M. Ajayan, J. Shen and M. Ye, *J. Mater. Chem. A*, 2018, **6**, 19417-19424.

23 H. Xu, J. Cao, C. Shan, B. Wang, P. Xi, W. Liu and Y. Tang, *Angew. Chem.*, 2018, **130**, 8790-8794.

24 Y. Guo, J. Tang, Z. Wang, Y.-M. Kang, Y. Bando and Y. Yamauchi, *Nano energy*, 2018, **47**, 494-502.

25 W. Fang, H. Hu, T. Jiang, G. Li and M. Wu, *Carbon*, 2019, **146**, 476-485.

26 F. Guo, H. Yang, L. Liu, Y. Han, A. M. Al-Enizi, A. Nafady, P. Kruger, S. Telfer and S. Ma, *J. Mater. Chem. A*, 2019, **7**, 3624-3631.

27 Y.-R. Hong, S. Mhin, K.-M. Kim, W.-S. Han, H. Choi, G. Ali, K. Y. Chung, H. J. Lee, S.-I. Moon and S. Dutta, *J. Mater. Chem. A*, 2019, **7**, 3592-3602.

28 Y. Liu, S. Jiang, S. Li, L. Zhou, Z. Li, J. Li and M. Shao, *Appl. Catal. B-Environ.*, 2019, **247**, 107-114.

29 L. An, J. Feng, Y. Zhang, R. Wang, H. Liu, G. C. Wang, F. Cheng and P. Xi, *Adv. Funct. Mater.*, 2019, **29**, 1805298.